MICROROBOTS

Coordinated behavior of autonomous microscopic machines through local electronic pulse coupling

Milad Taghavi[1]*†, Wei Wang[2,3,4]†, Kyubum Shim[1], Jinsong Zhang[2], Itai Cohen[2,4,5,6], Alyssa Apsel[1]

Increasingly functional microscopic machines are poised to have massive technical influence in areas including targeted drug delivery, precise surgical interventions, and environmental remediation. Such functionalities would increase markedly if collections of these microscopic machines were able to coordinate their function to achieve cooperative emergent behaviors. Implementing such coordination, however, requires a scalable strategy for synchronization—a key stumbling block for achieving collective behaviors of multiple autonomous microscopic units. Here, we show that pulse-coupled complementary metal-oxide semiconductor oscillators offer a tangible solution for such scalable synchronization. Specifically, we designed low-power oscillating modules with attached mechanical elements that exchange electronic pulses to advance their neighbor's phase until the entire system is synchronized with the fastest oscillator or "leader." We showed that this strategy is amenable to different oscillator connection topologies. The cooperative behaviors were robust to disturbances that scrambled the synchronization. In addition, when connections between oscillators were severed, the resulting subgroups synchronized on their own. This advance opens the door to functionalities in microscopic robot swarms that were once considered out of reach, ranging from autonomously induced fluidic transport to drive chemical reactions to cooperative building of physical structures at the microscale.

INTRODUCTION

Our world is full of breathtaking behaviors that arise from temporal coordination. Cardiomyocytes, the cells responsible for contraction of the heart, coordinate to produce temporally oscillating pressure gradients that sustain life. Fireflies engage in spectacular mating displays where synchronization of their chemically driven fluorescence creates a symphony of light. In humans, coordination is vital to the thrill of propagating the Mexican wave at stadiums as well as the construction of engineered systems ranging from skyscrapers to the electric grid.

Increasingly, the prospect of generating temporally coordinated emergent behaviors in microscopic robots is becoming a possibility. Currently available microrobot systems have already extended our ability to access and explore microscale environments that conventional machines and robots cannot reach (*1*–*5*). Moreover, advances in electronics fabrication, materials science, and heterointegration have led to increasingly functional autonomous microscopic robots that can, for example, locomote on their own or drive elementary fluid flows. Such robots are particularly intriguing for generating temporal coordination because it may be possible to design synchronization mechanisms into the electronic circuits that drive them. Implementing temporal coordination in microscopic systems would enable many new functionalities not currently available to the microscopic world, including communication, coordinated flow control over centimeter-scale surfaces, and the collective construction of structures.

Macroscale strategies for temporal coordination are often constraining or not viable at the microscale. In magnetically controlled microrobots, for example, it is difficult to achieve autonomy or changes in the relative phases of the robots once the system is fabricated. In electronic feedforward schemes used to synchronize macroscale electronic devices and networks, a master oscillator controls the synchronization state by sending out signals that other oscillator circuits can lock onto. Such schemes require high power consumption by the master oscillator and a method for sending the signals either through wires or via transmitters and receivers. At the microscale, however, the low power budget, the complexity associated with physical wiring, and the inability to transmit information wirelessly over long distances make such schemes very challenging to implement. Last, because of the limited circuit areas on these microscopic systems, timing must be controlled by electronic circuit elements rather than crystals. The phase of such oscillators tends to drift, and their exact frequency is sensitive to process variation during fabrication as well as environmental conditions. As such, sending sparse phase reset signals is not effective. One could imagine using a continuous optical clock signal, but this scheme would restrict the operation of the machines to line of sight and complicate the sending of commands to the individual units. Thus, implementing scalable synchronization at the microscale will require new strategies.

Here, we report a series of structures composed of modular micromachines that exhibit a scalable strategy for coordination of actuation using the mechanism of pulse coupling between complementary metal-oxide semiconductor (CMOS) oscillators (Fig. 1A). The primary innovation of this work lies in achieving synchronization in microscopic machines, a challenging task because of their small size and limited power. Our work demonstrates synchronization in microscopic robots equipped with onboard CMOS electronics, enabling them to exchange pulses and synchronize their cycles autonomously. This capability allows for the generation of wavelike collective behaviors, such as metachronal waves, which offer high fault tolerance (*6*, *7*). Unlike previous microrobot research (*3*–*5*, *8*, *9*), which relied on external control mechanisms like magnetic or electric fields, our autonomous synchronization provides a more advanced and versatile approach.

[1]Department of Electrical and Computer Engineering, Cornell University, Ithaca, NY, USA. [2]Laboratory of Atomic and Solid State Physics, Cornell University, Ithaca, NY, USA. [3]Sibley School of Mechanical and Aerospace Engineering, Cornell University, Ithaca, NY, USA. [4]Kavli Institute at Cornell for Nanoscale Science, Cornell University, Ithaca, NY, USA. [5]Department of Physics, Cornell University, Ithaca, NY, USA. [6]Design Technology, Cornell University, Ithaca, NY, USA.
*Corresponding author. Email: mt795@cornell.edu
†These authors contributed equally to this work.

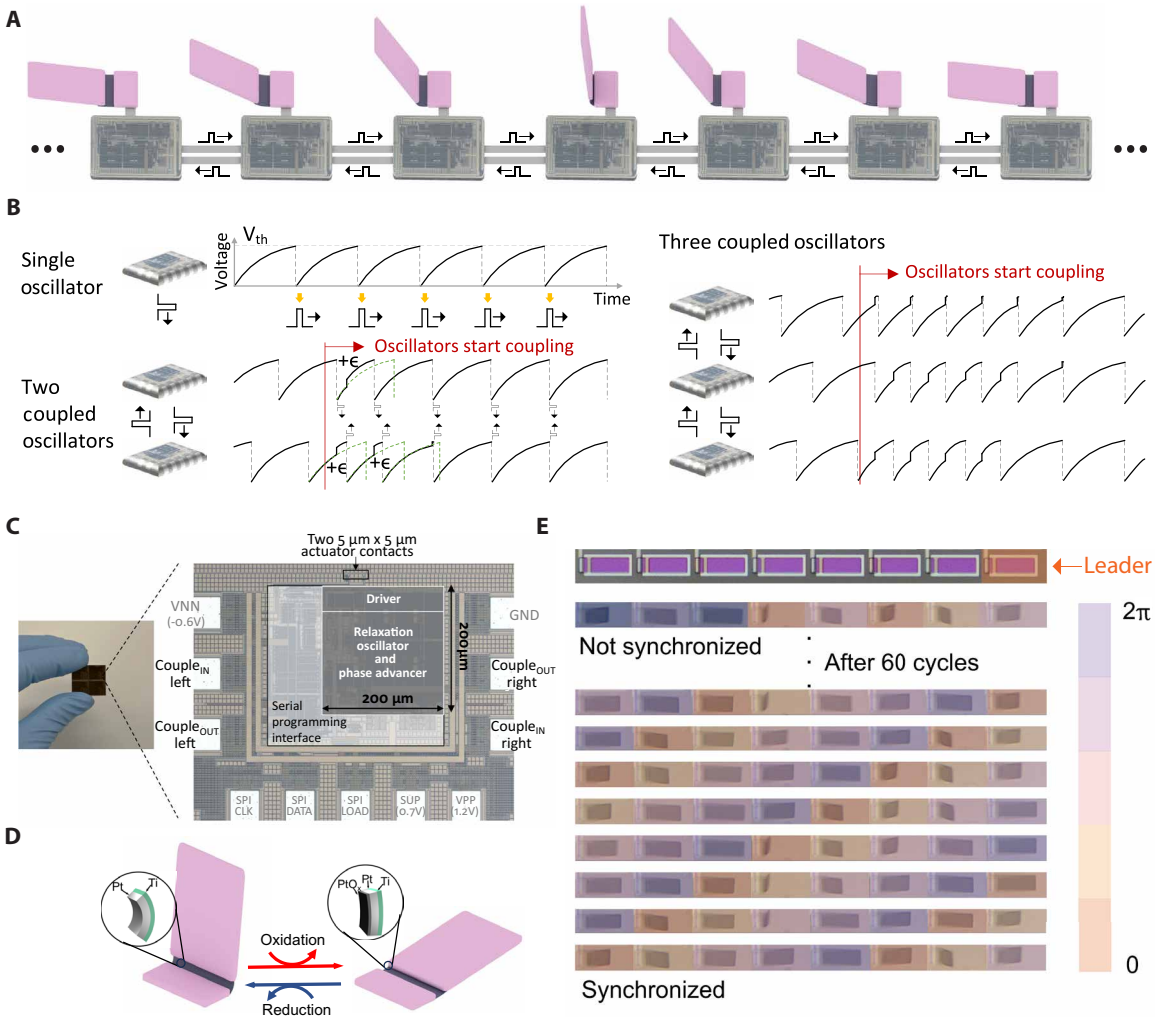

Fig. 1. Scalable synchronization of microscale robots. (**A**) Scheme for scalable synchronization strategy that uses pulse coupling between oscillators. (**B**) Pulse-coupled oscillators achieve synchronization by exchanging pulses. Each oscillator sends a pulse to its neighbors when it ends its cycle. When an oscillator receives a coupling pulse, it advances its state/voltage by a fixed amount, ϵ. The dashed green lines show the state progression in the absence of a coupling pulse. After several cycles, the oscillators synchronize. (**C**) Each fabricated module includes a relaxation oscillator, peripheral control circuitry, and a driver to interface and control up to two SEAs. The peripheral control circuitry controls the state of the oscillator and enables synchronization with two neighboring modules. (**D**) The bendable paddle comprises an active Pt layer (white) with a passive Ti layer (green). The hinge is delineated by the rigid SiO_2 panels (purple). Actuation is achieved through the expansion (+1.2 V) or contraction (−0.6 V) of the Pt surface at different applied voltages. (**E**) Demonstration of metachronal waves, a rudimentary synchronization behavior. Here, we connected the CMOS modules to separately fabricated paddles. To generate metachronal waves, we introduced time delays in the pulse transmission. The bending angles of the paddles correspond to the phases of the output voltage signals. The color map visually represents the phase in each paddle. In a system with eight modules, the initial state is unsynchronized. After 60 actuation cycles, however, we observed distinct metachronal wave patterns (see movie S1).

RESULTS

Scalable synchronization of microscale mechanical systems

In our scheme, each micromachine module consisted of a CMOS circuit attached to an electrically actuated paddle and could transmit and receive electrical pulses to and from its neighboring modules (Fig. 1A), although designs that allow for coupling to more neighbors are easily imagined. Because each module locally connected to only two neighbors, extension to additional modules would be trivial and would avoid complicated wiring schemes.

To implement scalable synchronization, we drew inspiration from Mirollo and Strogatz's model of biological pulse-coupled oscillators (*10*–*13*) (Fig. 1B). In our conceptualization, we designed our circuit modules to act as nonlinear electrical oscillators that transmitted phase-advancing voltage pulses to their neighbors when they reached a threshold voltage V_{th}. When a neighboring module received a voltage pulse, it advanced its state by a voltage change of ϵ. The oscillator nonlinearity guarantees that when modules are coupled, they will eventually synchronize (*12*, *13*). We show a conceptual schematic of how synchrony arises in two and three pulse-coupled oscillators in Fig. 1B. This strategy is scalable and allows for synchronization over arbitrarily long module chains. To implement this approach in our experiments, we fabricated pulse-coupling modules with a 180-nm CMOS process from our cooperative boundary X-FAB, as shown in Fig. 1C. Each module comprised a relaxation oscillator, a pulse generator, a phase advancer, and other supporting circuitry. These elements occupied a die area of approximately 200 µm by 200 µm and

consumed ~70 pW at 0.7 V. A serial programming interface was used to initialize the circuit, determine neighbor connections, and designate a leader. The leader designation was made by adjusting a capacitor to increase the oscillator frequency by ~5%. The periphery of the module was used for power supply, ground, and coupling to neighboring modules. Last, the driver amplified the core supply voltages to actuate the paddle (see Materials and Methods for details).

The paddle was driven by the recently developed surface electrochemical actuators (SEAs) (*14*–*17*). Briefly, each actuator was composed of a 7-nm-thick platinum (Pt) thin film, capped on one side by a passive layer of titanium (Ti) (Fig. 1D). Silicon dioxide (SiO_2) rigid panels (500 nm) were used to define the actuatable region. To induce actuation of these paddles in phosphate-buffered saline (PBS; 1×; pH 7.45), the potential was raised to approximately 1.2 V relative to the Ag/AgCl reference electrode, initiating the electrochemical oxidation of the exposed Pt surface without generating bubbles. This oxidation process caused the Pt surface to expand, leading to the flattening of the actuator (red path of Fig. 1D). By applying a voltage of approximately −0.3 V, the Pt film was reduced, returning the actuator to its initial state (blue path of Fig. 1D).

To demonstrate a synchronized metachronal wave, we connected a linear array of eight pulse-coupled modules, with a constant phase delay between them, and drove an array consisting of eight fabricated paddles (Fig. 1E and movie S1). To guarantee the reliability of the circuit, we used external wires to power and program the circuit. Because of the cost of fabrication, we separated the chips from the actuators and used external wires to connect them. We found that initially the paddles oscillated at random phase offsets because of the random initial conditions. After 60 cycles, however, we found that the paddles synchronized and exhibited notable metachronal waves with a phase delay of ~20% between neighboring paddles, with the leader "leading" the wave. Although synchronization was robust, it is subject to a number of system parameters as detailed in the literature (*18*), including coupling strength, pulse duration, delay, and blackout/refractory period, as well as the number of oscillators in the system. For example, insufficient coupling strength will prevent synchronization. Any large variations in the system, such as large variations in oscillator frequencies, as well as nonreciprocal settings, such as different coupling strengths between oscillators, can also be impediments in achieving synchronization. Last, topological alterations that break symmetry will impair synchronization. Our results showed that there exists a parametric space for achieving synchronization in micromechanical and microrobotic systems that is robust. Thus, our demonstration illustrated the possibility of implementing scalable synchronization in microscopic systems using distributed control, simple computation, and minimal wiring.

The pulse-coupling strategy

The key technological advance for achieving this synchronization is the design of the CMOS pulse-coupled oscillating modules with ultraslow oscillators matched to long mechanical timescales (Fig. 2). The relaxation oscillator and phase advancer architectures are highlighted by the blue and green dashed boxes shown in Fig. 2A. In the relaxation oscillator (blue dashed box), the circuit elements R1, R2, and R3 are analogous to the stages of a loop of inverters, a common strategy for implementing a relaxation oscillator using circuit elements. We used dynamic leakage suppression (DLS) gates (*19*, *20*) instead of standard CMOS gates to construct these circuit elements. This strategy allowed for similar operations using only picoamperes of current. The low currents reduced power consumption and had the added benefit of increasing the timescale associated with the charging of capacitance internal to the relaxation oscillator. The internal capacitor could be kept small, and the resulting frequency was in the 100- to 0.1-Hz range necessary for driving mechanical devices. When $Reset_A$ and $Reset_B$ were zero, the NOR gates l_1,l_2 acted as input-output shorted inverters that shunted the current through the capacitor. The voltage over the capacitor V_{AB} held the state of oscillation. V_{AB} was composed of two concave down signals followed by two concave up signals whose timescales are set by the circuit capacitance C and pull-down/up paths of l_1,l_2 NOR gates (see the "Concave-up discharge" section in the Supplementary Materials for details). Buffering the output of the R2 stage gave an oscillating clock signal, with the high and low state of the clock corresponding to the rising and falling transitions of V_{AB} (Fig. 2A, right schematic).

To alter the oscillation state, we used a phase advancer (green dashed box) to more rapidly discharge either node A or B. For example, when the $Couple_{IN}$ aligned with clock high (Fig. 2B), the NOR gate l_1 acted as an inverter that shunted the current through the capacitor whereas l_2 added an additional discharge path to ground (see the equivalent circuit model on the right). The additional discharge pathway lowered V_B (orange arrow), which, in turn, increased V_{AB} (green arrow) and advanced the phase of the oscillator. Conversely, when the $Couple_{IN}$ aligned with clock low (Fig. 2C), the NOR gate l_1 added an additional discharge path to ground, and l_2 shunted the current through the capacitor (see the model on the right). Here, the additional discharge pathway lowered V_A, which, in turn, decreased V_{AB}. Because this voltage decrease occurred as V_{AB} was falling, the oscillator phase was once again advanced.

In testing the fabricated CMOS circuit, we found that, regardless of arrival time (t), the voltage pulses ($Couple_{IN}$) advanced the oscillator phase. We show the phase response curve (PRC) versus arrival time in Fig. 2D. Here, the PRC is defined as the change in period induced by the incoming couple ($T - T^*$), normalized by the original clock period, T. The plot indicates that PRC is always positive and that the lowest phase advance happens at the middle and end of the cycle when the coupling pulses are emitted. These two characteristics dictate that the module clock phases will synchronize to the oscillator with the fastest frequency.

Coupling scheme and synchronization quality

We found that oscillator pairs could synchronize once the coupling was bidirectional so that we obtained a closed loop with feedback. To generate metachronal waves, a rudimentary behavior requiring synchronization, we implemented a phase delay Δ between the oscillators by introducing a refractory period over which the oscillator was insensitive to the incoming couple (see the "Refractory period" section in the Supplementary Materials for details). We show the dynamics of the oscillator frequencies and phases in Fig. 3 (A and B). When the coupling was only feedforward or unidirectional, we found that the follower module frequency (orange) approached that of the leader (blue) within ~30 cycles but always remained slightly lower (blue shaded region). This consistently negative mismatch contributed to a phase drift as shown in the figure inset. Once the coupling was bidirectional, however, the follower module frequency locked onto that of the leader, and a stable phase delay Δ was observed (Fig. 3B). We found that the relative jitter defined as the normalized difference between the follower and leader periods, $\left(T_{F_i} - T_{L_i}\right) / T_{L_i}$, gave a variance of less than 0.1%, indicating excellent synchronization between

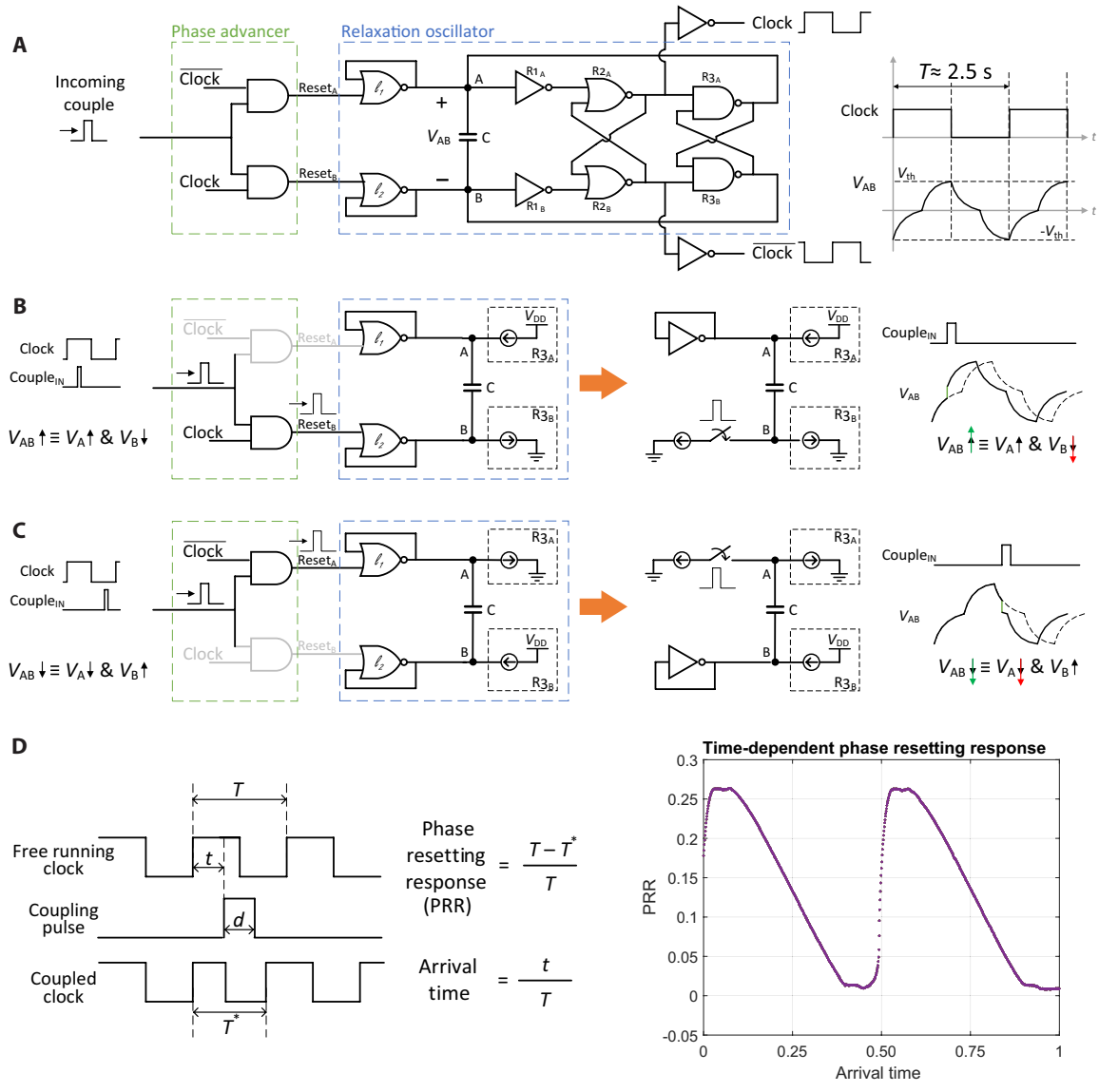

Fig. 2. The pulse-coupling strategy. (**A**) Each module includes a relaxation oscillator (R1, R2, and R3), constructed using DLS gates (*19*, *20*). In this architecture, V_{AB} holds the state of oscillation. Here, the high and low states of the clock correspond to the rising and falling of V_{AB}. On the basis of this correlation, the phase advancer directs the incoming pulse through upper or lower paths to advance the state of oscillation in response to coupling. When no couple is available, $Reset_A$ and $Reset_B$ are at logic low. Under this condition, one input of the NOR gates is grounded, and it can be simplified to an inverter. Here, the connection of input to output creates a variable resistance. This resistance with the parallel capacitance creates the concavity conditions required for the state function of pulse-coupled oscillators. (**B**) If the incoming pulse arrived during the high state of the clock, we sped up the rise of V_{AB} by discharging node B through the lower path. (**C**) If the incoming pulse arrived during the low state of the clock, we sped up the fall of V_{AB} by discharging node A through the upper path. (**D**) The oscillator achieves an all-positive, nonuniform phase response over the full range of its period, which is required for synchronization.

the modules. Although we observed minor low-amplitude and high-frequency oscillations in the circuits, we found that these damped out in the paddles, which acted as low-pass filters. Moreover, this frequency locking was robust (we experimentally demonstrated synchronization, loss of synchrony, and resynchronization in movie S2) and could be sustained over hundreds of thousands of cycles (Fig. 3C).

Scalability and network expansion

We found that this strategy was easily scalable and could be implemented in longer arrays of oscillators, which, when coupled to the mechanical elements, could be used to generate desired complex actuation patterns (Fig. 4). We simply added two connecting wires that enabled adjacent modules to exchange coupling pulses (Fig. 4A). We found that the frequency synchronization occurred in stages where subsets of oscillators synchronized before lastly locking onto the leader, which, for eight oscillators (OSCs 1 to 8), occurred after roughly 75 cycles. These dynamics could also be observed in the phase difference between the modules where synchronization manifested as parallel curves. We found that nodes synchronized with their highest-frequency neighbors. In this particular example, OSCs 4 to 8 synchronized with each other before synchronizing with the leader, OSC 1. Similar synchronization dynamics were observed when the array

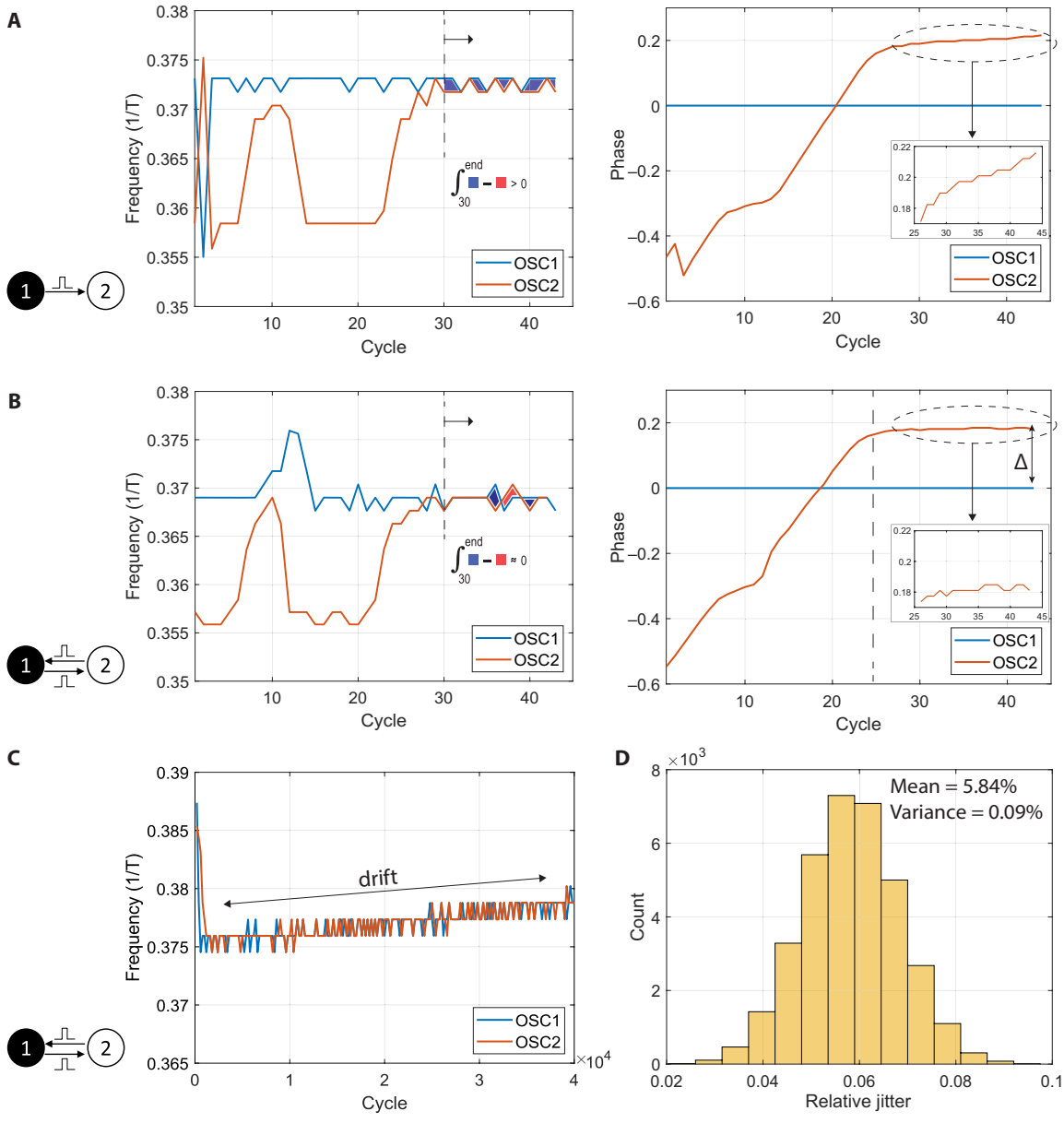

Fig. 3. Coupling scheme and synchronization quality. (**A**) Frequency and phase dynamics of two oscillators with unidirectional connectivity. Here, only the leader (OSC 1) sends couples to the follower (OSC 2). With this mode, modules synchronize with an average error in frequency, in which the frequency from the follower is always lower than the frequency of the leader. The integral of this frequency error grows in time, leading to a slow drift in the relative phase of the follower with respect to the leader. (**B**) Frequency and phase dynamics of two oscillators with bidirectional coupling. The integral of frequency error between leader and follower is negligible, and the oscillators synchronize with precise frequency matching and maintain a fixed phase difference after synchronization. (**C**) The coupling counteracts the frequency drift, and oscillators remain synchronized over 24 hours after more than 4×10^5 cycles. (**D**) The follower tracks the cycle-to-cycle variation of the leader and achieves a relative jitter with a mean of ~6% and a variance of 0.09%.

was expanded to 16 oscillators (Fig. 4B). In addition, the phase delay between the oscillators was tunable. We experimentally verified that for phase delays of 16% and 20%, the coupled oscillators could be synchronized to the exact same frequency (see fig. S1). Overall, we found that synchronization yielded a consistent phase offset (orange), negligible duty cycle distortion for the follower clocks (yellow), and a cycles-to-synchronization count that increased linearly with the module count (gray). We show the final sequentially synchronized clock pulses from all 16 modules in Fig. 4C. We found a consistent phase difference between adjacent modules of ~20%, demonstrating a wavelike pattern in the module array.

These wavelike patterns can be used to generate complex actuation sequences. To demonstrate an example of such a sequence, we fabricated a microscopic machine consisting of 16 paddles arranged in a cross configuration. We then wired each paddle to one of the modules in the synchronizing array. The wavelike pattern shown in Fig. 4C was then translated to a complex synchronized actuation cycle (Fig. 4D and movie S3). Here, the arrows in the figure show the

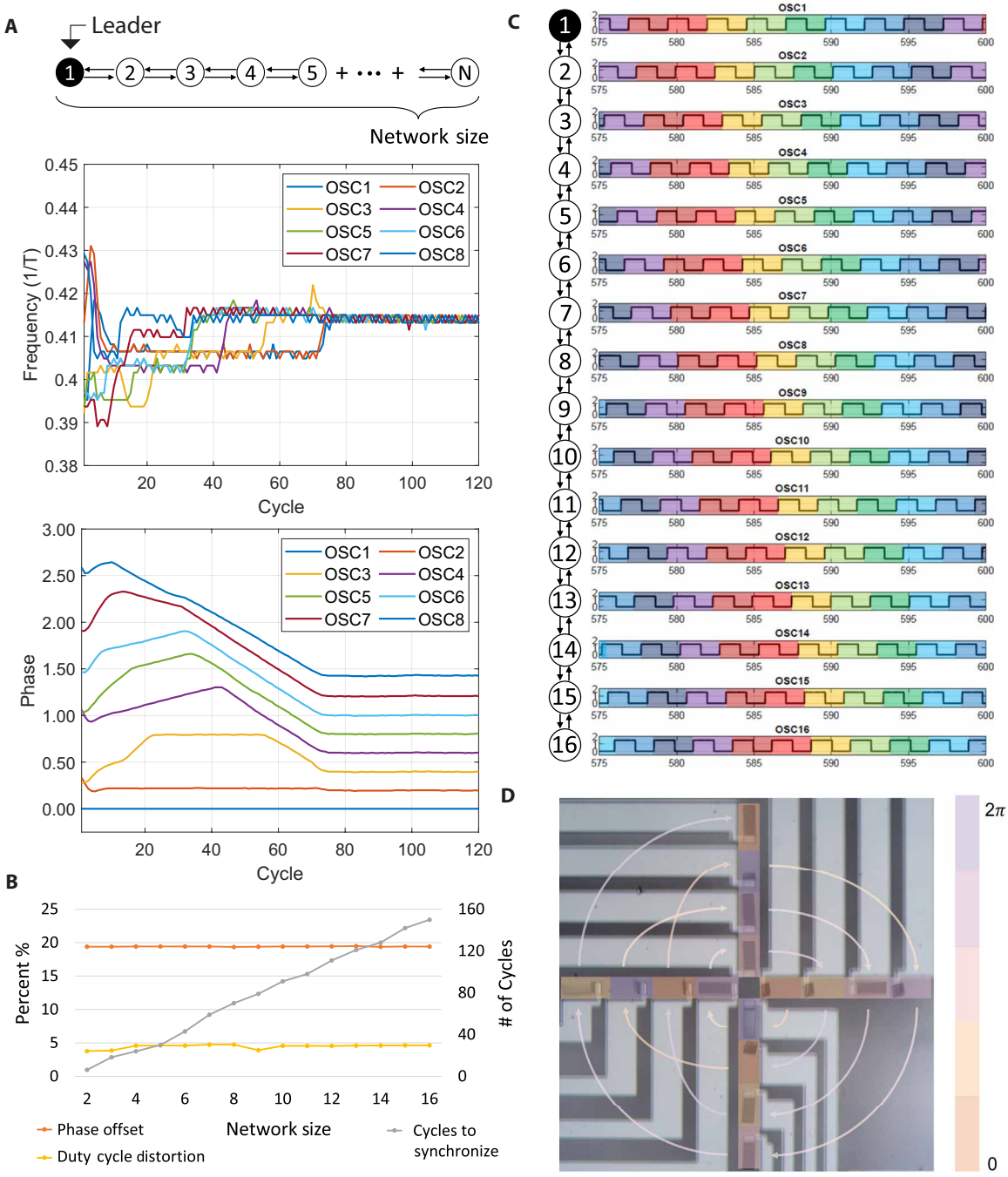

Fig. 4. Scalability and network expansion. (**A**) Phase and frequency dynamics of eight coupled oscillators. We found that the oscillators synchronized with the leader, reaching stable synchronization by the 75th cycle. We found that local synchronization with uniform phase differences preceded the final synchronized state. (**B**) Such synchronization is easily expanded to 16 pulse-coupled oscillators. The oscillators maintained 19% phase differences. Coupling had minimal impact on duty cycle (<5%), averaged over 10 iterations. We found that the number of cycles needed to synchronize a linear network grew with the number of oscillators. (**C**) Sequential synchronization for 16 modules with module 1 as the leader. (**D**) Two-dimensional metachronal wave propagation in a micropaddle structure controlled by 16 pulse-coupled modules with a bidirectional line network; arrows indicate connections, and semitransparent colors represent phases (see movie S2).

order of connectivity of the modules. We found that with each step or arrow, the phase of the paddle bending cycle advanced by ~20% (or one color gradation). This motif is only one example of what can be achieved by coupling 16 modules in an array. Linearly extending this network is a trivial example that would allow for the synchronization of a larger number of oscillators. Another extension, which would require more complex wiring during fabrication, would be to change the number of neighbors each oscillator has. Such higher connectivity would also enable faster synchronization. However, even by exploiting the flexibility and modularity of the nearest-neighbor

pulse-coupled nodes already fabricated here, we were able to experimentally demonstrate a number of additional actuated behaviors as well, including synchronization to different leaders (fig. S2 and movie S2), synchronization of loop structures (fig. S3 and movie S4), and wave propagation in synchronized four-by-four arrays (movie S5). We note that these topologies only required nearest-neighbor coupling to achieve synchrony and a range of wavelike behaviors, rather than the all-to-all coupling contemplated in the Strogatz model. Collectively, these results highlight the scalability of our approach.

Robustness and stability

The pulse-coupled oscillators were robust. For example, when an array of eight synchronized modules was disrupted by a scrambling voltage shock, which caused a reset in the phase of the modules, and randomly reinitialized the states of oscillation for each, we found that they were able to synchronize once again at the same leader frequency (Fig. 5A). From measurements of the phase, we observed that the dynamics after disturbance exhibited similar timescales and patterns to the initial synchronization dynamics. For example, we observed that OSCs 6 to 8 tended to locally synchronize with each other before they joined the group and locked onto the leader module. Formally, such robustness is expected because, mathematically, the oscillators implemented a period-1 solution (*21*). These results indicate that this synchronization strategy was resilient and could withstand noisy environments.

In addition, such networks can maintain their synchronization capabilities even when local connections are severed. For example, we show that when an array of eight oscillators that have achieved synchronization was broken into two subarrays, each array achieved internal synchronization with the fastest oscillator in its group (Fig. 5B). More specifically, when the coupling path between modules 5 and 6 was severed at the ~110th cycle, the array broke into two subarrays, with OSCs 1 to 5 locking onto OSC 1 and OSCs 6 to 8 locking onto OSC 6 at a slightly lower frequency. These dynamics can be seen in the plot of the phase versus cycle. Here, we found that although the phases of OSCs 1 to 5 were similar before and after severing, the phases of OSCs 6 to 8 drifted with respect to OSC 1 but remained parallel. This can be illustrated more clearly by subtracting the phase of the leader (OSC 6) and offsetting these curves by −1 (see curves for OSC 6, OSC 7, and OSC 8). Such breaks in the topology could be programmed, enabling us to break up or join separate elements depending on the desired function of the entire system.

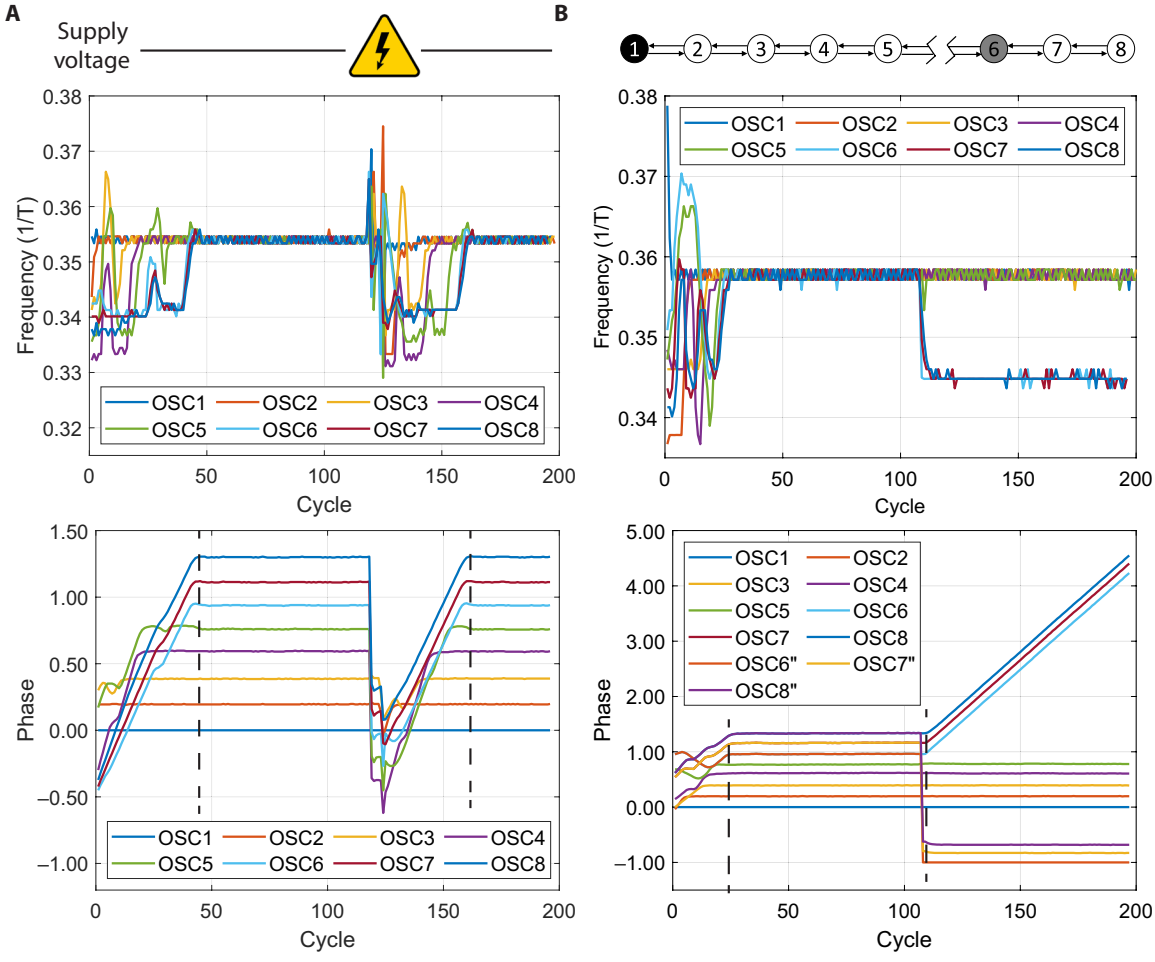

Fig. 5. Robustness and stability. (**A**) The eight modules synchronized by the 50th cycle; a momentary change in the supply voltages caused the modules to lose synchronization. The modules are able to recover the stable synchronized state and position themselves within a 20% phase difference with their neighbors. (**B**) In the incident of a network discontinuity, the modules in the subnetworks follow their new regional leader. In this test, the connection between modules 5 and 6 was severed. We found that modules 6, 7, and 8 remained synchronized with 6 as their leader.

Alternative wavefronts

Alternative wavefronts can be achieved by changing the leader oscillator and connection topology. For example, in a linearly connected oscillation topology, we could get synchronized oscillations with the leader at one edge, in the middle, and at both edges (fig. S2 and movie S2). In addition, we showed that a loop consisting of eight oscillators can be synchronized (fig. S3 and movie S4). When OSC 1 was set to be the leader, the wave started at OSC 1 and then propagated forward and met at the far end. When both OSC 1 and OSC 8 were set as the leader, the wave propagated from oscillators 1 and 8.

Last, because the couple-in and couple-out signals were digital, we could split them to enable connections to additional neighbors so that this synchronization strategy could be implemented in a wide variety of network topologies. To demonstrate this possibility, we abstracted the RC nature of each relaxation oscillator (*12*) and simulated the synchronization process across a large number of pulse-coupled oscillators. Here, we modeled the phase response for each oscillator as $1 - be^{b\Phi} / \left(e^{b} - 1\right)$, with b representing the concavity of the function. We then integrated the oscillators into a time series simulator using custom MATLAB code that is accessible in Zenodo. Adding two additional neighbors enabled us to create a node with four synchronized branches (Fig. 6A). When combined with a closed-loop architecture (Fig. 6B), we could construct synchronized states in a nested loop topology with 16 nodes (Fig. 6C and movie S6). Such nested structures enable the generation of five loops that show bidirectional metachronal propagation, with the middle loop connecting the other four loops. Moreover, these patterns can be completely reorganized by choosing different leading oscillators. Last, the motif in Fig. 6A could be tiled in a scalable manner as illustrated by the 10-by-10 lattice structure in Fig. 6 (D and E). Here, too, different oscillation patterns could be achieved depending on which leader nodes were selected. When the bottom left node was designated leader (Fig. 6D and movie S7), we observed a metachronal wave traveling from the bottom left to the top right. When both the bottom left and top right oscillators were set as the leaders (Fig. 6E and movie S8), the metachronal waves originating from both the bottom left and top right merged along the pattern's diagonal midline. As these examples illustrate, electronic selection of the leader nodes along with programming of the network connectivity enabled a combinatorially large number of propagation

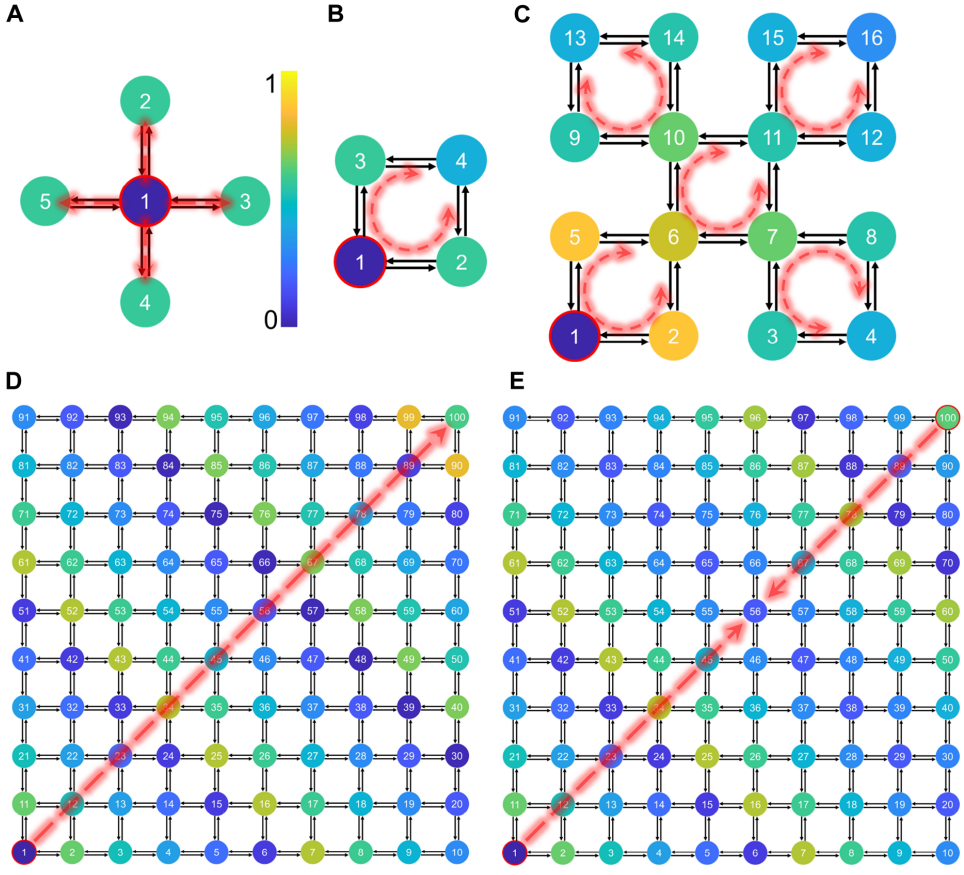

Fig. 6. Alternative wavefronts. (**A**) Synchronized phases of five oscillators connected in a branched configuration. We programmed the middle oscillator, marked with a red circle, as the leader. The semitransparent dashed lines with red arrows indicate the wave propagation. Phases were mapped to colors using a Parula color map. (**B**) Synchronized phases of a rectangle loop with the bottom left oscillator as the leader. The metachronal wave originates from the leader, propagates to both sides, and merges at the other end of the loop. (**C**) Synchronized phases of a nested loop with the bottom left oscillator as the leader. This network forms five loops, with bidirectional metachronal waves. (**D**) Synchronized phases of a 10-by-10 oscillator array connected as a rectangle lattice network with the bottom left oscillator as the leader; the metachronal wave propagates from the bottom left to the top right of the network along the diagonal direction (see movie S4). (**E**) Synchronized phases of a 10-by-10 oscillator array with the bottom left and top right oscillators as the leaders; the metachronal wave starts from the bottom left and the top right and propagates along the diagonal direction and merges in the middle (see movie S5).

patterns without any physical modifications to the micromachines. As such, this approach provides a very powerful method for generating numerous actuation patterns.

DISCUSSION

Collectively, these results illustrate that pulse coupling is a powerful method for implementing scalable low-power synchronization and coordinated behaviors in microscopic machines and ultimately robots. The implications of this breakthrough are vast. Without coordination, robot swarms cannot sequence tasks and are rendered hapless, unable to understand each other's language. With coordination, however, one can foresee a future in which robots both tethered, as shown here, and mobile will be able to perform and even surpass the emergent behaviors demonstrated by insects, microorganisms, and even biological tissues. Local coupling between segments of a single robot would enable central pattern generators that can lead to complex motions and behaviors such as locomotory gaits, grasping, and environmental manipulation. In microscopic robot swarms that couple wirelessly via antennas, such synchronization could generate emergent behaviors impossible to achieve with a single robot. For example, surfaces covered with robotic cilia could act as tiny laboratories, sensing their chemical environment, mixing chemicals together, transporting reaction intermediates, and separating out reaction products for analysis, like many tiny hands sorting molecules. Such processes could be driven through manipulation of the phase differences, the leader nodes, and the network connectivity in this expansive experimental platform capable of synchronization.

MATERIALS AND METHODS

Driver circuit

The actuators required a drive voltage range of −0.3 to 1.2 V, which is different from the core voltage range of 0 to 0.7 V for the electronics. The circuit in fig. S4A shows the circuit that we used to implement this level shifting. The function of the circuit is as follows: When the signal from the core oscillator was at 0 V, it turned off P_1 ($V_{SG} = 0$), whereas P_2 turned on ($V_{SG} > V_{thp}$). This, in turn, set the output voltage to top rail (V_{PP}), which turned on N_1 ($V_{GS} > V_{thn}$). As N_1 turned on, it biased the gate voltage of N_2 at −0.3 V and turned off N_2 (fig. S4B). On the other hand, when the signal from the core oscillator was at 0.7 V, it turned off P_2 because the source-gate voltage of this p-channel MOSFET (metal-oxide-semiconductor field-effect transistor) could only reach the threshold voltage and could not conduct. The 0.7 V, however, turned on P_1 because it caused a source-gate voltage above its threshold voltage ($V_{SG} > V_{thp}$). As P_1 turned on, it biased the gate voltage of N_2 above the threshold voltage, which set the output voltage to the bottom rail (V_{NN}), which, in turn, set the gate-source voltage of N_1 to zero and turned it off (fig. S4C).

Fabrication process

Making the micropaddles requires fabrication of five material layers. These include, from bottom to top, growing and patterning the releasing layers; growing and etching 0.5-μm-thick rigid SiO_2 panels; fabricating 3-nm Ti followed by 7-nm Pt layers for the actuator; patterning the wire bonding pads; bonding the pads to the chip carrier; and etching the release layers to free the paddles. The detailed recipe is as follows.

Releasing layer

A release layer of 180-nm aluminum was deposited on SiO_2 wafers using an E-beam evaporator (CVC SC4500). To protect this release layer during fabrication, an additional 30-nm Al_2O_3 was grown at 110°C using atomic layer deposition (ALD) by OXFORD ALD FlexAL. To pattern these release layers, a positive photoresist (Microposit S1813) was spin-coated and exposed using an ABM contact aligner, and the wafer was then developed in a developer (MicroChemicals AZ 726 MIF). The exposed release layers were etched by the aluminum etchant type A at 40°C. Then, the photoresist was stripped using Microposit Remover 1165 with sonication, followed by oxygen plasma cleaning for 3 min (Oxford PlasmaLab 80+).

SiO_2 panel

SiO_2 (500 nm) was grown using Oxford 100 PECVD. Positive photoresist S1813 was spin-coated and patterned. The SiO_2 was etched using CHF_3/O_2 recipe (Oxford 80+ etcher). Then, the photoresist was stripped in Microposit Remover 1165.

Ti and Pt layers

Ti (3 nm) was sputtered onto the sample at 3 mtorr and 400 W (AJA sputter tool). Then, a 7.5-nm Pt layer was grown using ALD (Veeco Savannah ALD) at 175°C. The positive photoresist S1813 was spin coated and patterned. The Ti and Pt layers were then etched by an ion mill tool at 600 V (AJA ion mill). Then, the photoresist was stripped in Microposit Remover 1165.

Interconnect

A negative photoresist (MicroChemicals NLOF 2020) was spin coated and patterned. Ti and Pt (100 nm), functioning as pads for wire bonding, were sputtered at 3 mtorr and 400 W (AJA sputter tool). The photoresist was stripped with Microposit Remover 1165 with sonication.

Wire bonding

The paddles were then packaged into a chip carrier with DIP (CSB06428D) from Spectrum using aluminum wires via wire bonding (Westbond 7400A Ultrasonic Wire Bounder). The aluminum wires were protected by optical adhesive (NOA 88 from Norland Products Inc.).

Releasing

The paddles were released using 5% TMAH solvent.

Experimental setup

The experimental setup included wire bonding the oscillators, connecting the oscillators with the actuators, and recording the actuation of the actuators under microscopes. The detailed process is as follows: First, the oscillators were packaged into a chip carrier with DIP (CSB06428D). Then, the packaged paddles and oscillators were inserted into the breadboard. The oscillators' outputs were connected to the paddles from the breadboard. Next, the oscillators were powered using an external power source and programmed through a serial programming interface with an FPGA chip. Last, a reflective microscope from Mitutoyo, integrated with a video camera, was used to record the actuation of the paddles.

Supplementary Materials

The PDF file includes:

Methods
Figs. S1 to S7
References (*23*–*26*)

Other Supplementary Material for this manuscript includes the following:

Movies S1 to S8

REFERENCES AND NOTES

1. B. Jurado-Sánchez, J. Wang, Micromotors for environmental applications. A review. *Environ. Sci. Nano* **5**, 1530–1544 (2018).
2. F. Mushtaq, X. Chen, S. Staufert, H. Torlakcik, X. Wang, M. Hoop, A. Gerber, X. Li, J. Cai, B. J. Nelson, S. Pané, On-the-fly catalytic degradation of organic pollutants using magneto-photoresponsive bacteria-templated microcleaners. *J. Mater. Chem. A* **7**, 24847–24856 (2019).
3. B. J. Nelson, I. K. Kaliakatsos, J. J. Abbott, Microrobots for minimally invasive medicine. *Ann. Rev. Biomed. Eng.* **12**, 55–85 (2010).
4. S. Palagi, P. Fischer, Bioinspired microrobots. *Nat. Rev. Mater.* **3**, 113–124 (2018).
5. M. Sitti, Voyage of the microrobots. *Nature* **458**, 1121–1122 (2009).
6. B. Chong, J. He, S. Li, E. Erickson, K. Diaz, T. Wang, D. Soto, D. I. Goldman, Self-propulsion via slipping: Frictional swimming in multilegged locomotors. *Proc. Natl. Acad. Sci. U.S.A.* **120**, e2213698120 (2023).
7. B. Chong, J. He, D. Soto, T. Wang, D. Irvine, G. Blekherman, D. I. Goldman, Multilegged matter transport: A framework for locomotion on noisy landscapes. *Science* **380**, 509–515 (2023).
8. B. R. Donald, C. G. Levey, C. D. McGray, I. Paprotny, D. Rus, An untethered, electrostatic, globally controllable mems micro-robot. *J. Microelectromechanical Syst.* **15**, 1–15 (2006).
9. W. Hu, G. Zhan Lum, M. Mastrangeli, M. Sitti, Small-scale soft-bodied robot with multimodal locomotion. *Nature* **554**, 81–85 (2018).
10. S. Bottani, Pulse-coupled relaxation oscillators: From biological synchronization to self-organized criticality. *Phys. Rev. Lett.* **74**, 4189–4192 (1995).
11. M. D. Greenfield, J. Schul, Mechanisms and evolution of synchronous chorusing: Emergent properties and adaptive functions in *Neoconocephalus* katydids (Orthoptera: Tettigoniidae). *J. Comp. Psychol.* **122**, 289–297 (2008).
12. R. E. Mirollo, S. H. Strogatz, Synchronization of pulse-coupled biological oscillators. *SIAM J. Appl. Math.* **50**, 1645–1662 (1990).
13. S. H. Strogatz, I. Stewart, Coupled oscillators and biological synchronization. *Sci. Am.* **269**, 102–109 (1993).
14. Q. Liu, W. Wang, M. F. Reynolds, M. C. Cao, M. Z. Miskin, T. A. Arias, D. A. Muller, P. L. McEuen, I. Cohen, Micrometer-sized electrically programmable shape-memory actuators for low-power microrobotics. *Sci. Robot.* **6**, eabe6663 (2021).
15. M. Z. Miskin, A. J. Cortese, K. Dorsey, E. P. Esposito, M. F. Reynolds, Q. Liu, M. Cao, D. A. Muller, P. L. McEuen, I. Cohen, Electronically integrated, mass-manufactured, microscopic robots. *Nature* **584**, 557–561 (2020).
16. M. F. Reynolds, A. J. Cortese, Q. Liu, Z. Zheng, W. Wang, S. L. Norris, S. Lee, M. Z. Miskin, A. C. Molnar, I. Cohen, P. L. McEuen, Microscopic robots with onboard digital control. *Sci. Robot.* **7**, eabq2296 (2022).
17. W. Wang, Q. Liu, I. Tanasijevic, M. F. Reynolds, A. J. Cortese, M. Z. Miskin, M. C. Cao, D. A. Muller, A. C. Molnar, E. Lauga, P. L. McEuen, I. Cohen, Cilia metasurfaces for electronically programmable microfluidic manipulation. *Nature* **605**, 681–686 (2022).
18. X. Y. Wang, R. K. Dokania, A. Apsel, PCO-based synchronization for cognitive duty-cycled impulse radio sensor networks. *IEEE Sens. J.* **11**, 555–564 (2010).
19. O. Aiello, P. Crovetti, L. Lin, M. Aliot, A pW-power Hz-range oscillator operating with a 0.3–1.8-V unregulated supply. *IEEE J. Solid State Circuits* **54**, 1487–1496 (2019).
20. D. Bol, R. Ambroise, D. Flandre, J.-D. Legat, Building ultra-low-power low-frequency digital circuits with high-speed devices, in *2007 14th IEEE International Conference on Electronics, Circuits and Systems* (IEEE, 2007), pp. 1404–1407.
21. P. C. Bressloff, S. Coombes, Travelling waves in chains of pulse-coupled integrate-and-fire oscillators with distributed delays. *Phys. D Nonlinear Phenom.* **130**, 232–254 (1999).
22. M. Taghavi, K. Shim, W. Wang, Delay locked synchrony in populations of pulse coupled oscillators (2023); https://zenodo.org/records/10392741.
23. A. Apsel, X. Wang, R. Dokania, *Design of Ultra-Low Power Impulse Radios*, vol. 124 of *Analog Circuits and Signal Processing* (Springer Science & Business Media, 2014).
24. G. Buzsaki, A. Draguhn, Neuronal oscillations in cortical networks. *Science* **304**, 1926–1929 (2004).
25. R. Olfati-Saber, J. A. Fax, R. M. Murray, Consensus and cooperation in networked multi-agent systems. *Proc. IEEE* **95**, 215–233 (2007).
26. S. H. Strogatz, Exploring complex networks. *Nature* **410**, 268–276 (2001).

Acknowledgments: We thank P. Chaudhari, H, Sinhmar, S. Maiti, I. Griniasty, I. Bukreyev, and T. Tapen for valuable discussions and T. Pennell, J. Clark, and G. Bordonaro for technical support. We wish to recognize the substantial contributions of graduated PhD students from the A. A. research laboratory over the past decade. Special acknowledgment goes to I. Bukreyev, E. Gantsog, and X. Wang for their commendable efforts in developing the pulse-coupling MATLAB time series simulator. **Funding:** This work was supported by the National Science Foundation (NSF; EFRI C3 SoRo-1935252), the US Army Research Office contract (W911NF-23-1-0212), the Cornell Center for Materials Research (DMR-1719875), and the Kavli Institute at Cornell for Nanoscale Science. This work was performed, in part, at the Cornell NanoScale Facility, a National Nanoscale Coordinated Infrastructure member supported by NSF grant NNCI-2025233. **Author contributions:** M.T., W.W., I.C., and A.A. conceived the project. M.T. designed the circuit and theory of operation. W.W. designed and fabricated the micropaddles. M.T., W.W., K.S., and J.Z. tested the circuit performance and paddle actuations. M.T., W.W., and K.S. performed the simulation and pattern for alternative wavefronts. All authors contributed to the writing of the manuscript. **Competing interests:** I.C. is an inventor on a patent application (PCT/US2021/021419) submitted by Cornell University that covers electrically programmable microscale shape-memory actuators and related robotic devices. W.W. and I.C. are inventors on a provisional patent application (63/267,190) submitted by Cornell University that covers actuators and control electronics for cilia metasurfaces and a provisional patent application (63/368,751) submitted by Cornell University that covers integrated circuits for controlling microscopic robots. All other authors declare that they have no competing interests. **Data and materials availability:** All code and various plots of wavefronts are available on Zenodo. They can be accessed at the following link: https://zenodo.org/records/10392741 (*22*). The MATLAB code constructs and simulates how a population of pulse-coupled oscillators will synchronize given sufficient time. The code builds off the framework listed in (*12*) by modeling each oscillator with respect to time as a nonlinear function. Control over the populations of oscillators and the connections between them, as well as pulse delays, effective coupling strength, and much more are provided as well.

Submitted 30 December 2023
Accepted 31 October 2024
Published 27 November 2024
10.1126/scirobotics.adn8067

Science Robotics

Coordinated behavior of autonomous microscopic machines through local electronic pulse coupling

Milad Taghavi, Wei Wang, Kyubum Shim, Jinsong Zhang, Itai Cohen, and Alyssa Apsel

Sci. Robot. **9** (96), eadn8067. DOI: 10.1126/scirobotics.adn8067

Editor's summary
In nature, coordinated behaviors occur among various groups of organisms. Achieving similar synchronization and coordination in microscopic devices and robots could open new possibilities in their functionality. Taghavi *et al.* demonstrated autonomous synchronization in low-power oscillating modules made from pulse-coupled complementary metal oxide semiconductor oscillators that can enable wavelike collective behaviors. The authors showed that the connected oscillators could exchange electronic pulses until the system was synchronized and that they were robust to external disturbances or individual oscillator failure. —Amos Matsiko

Science Robotics (ISSN 2470-9476) is published by the American Association for the Advancement of Science. 1200 New York Avenue NW, Washington, DC 20005. The title *Science Robotics* is a registered trademark of AAAS.